A&A 622, A45 (2019)
https://doi.org/10.1051/0004-6361/201833858

Astronomy & Astrophysics

High-velocity equatorial mass ejections and some other spectroscopic phenomena of the symbiotic star CH Cygni in an active stage⋆

T. Iijima[1], H. Naito[2], and S. Narusawa[3]

[1] Astronomical Observatory of Padova, Asiago Section, Osservatorio Astrofisico, 36012 Asiago (Vi), Italy
e-mail: takashi.iijima@oapd.inaf.it
[2] Nayoro Observatory, 157-1 Nisshin, Nayoro, Hokkaido 096-0066, Japan
[3] Nishi-Harima Astronomical Observatory, Hyogo Prefectural University, Sayo-cho, Hyogo 679-5313, Japan

Received 15 July 2018 / Accepted 26 November 2018

ABSTRACT

Context. CH Cyg is one of the most studied symbiotic stars. Its properties, however, are still not well known. Two main periods, about 15 years and 750 days, are known in the photometric and spectroscopic variations, and two models are proposed for these origins. One is a binary system with an orbital period of 15 years consisting of a hot component and pulsating red giant with a 750-day period. The other is a triple system consisting of an inner symbiotic binary with an orbital period of about 750 days and third component with an orbital period of 15 years. Several active stages have been observed since the 1970s during which the object brightened up by ΔU = 3−5 mag and prominent emission lines appeared. Large mass outflows were observed at some active stages.
Aims. The spectral variation of CH Cyg has been monitored at Asiago Observatories to understand the problems mentioned above. We have analysed spectra obtained in the time period from 1995 to 2004 which covers an active stage during the years 1998–2000.
Methods. High- and low-resolution optical spectra obtained at the Asiago Observatories are used.
Results. Narrow absorption lines of Fe I, Cr I, Ti I, and so on appeared in 1998 at an early phase of the active stage. These lines are clearly distinguished from those of the M-type giant and are typically found on the spectrum of early A-type dwarfs. They were redshifted by about 30 km s^{-1} with respect to the absorption lines of the M-type giant. Assuming that their radial velocities represent the orbital motion of the hot component, its semi-amplitude is estimated to be 37.0 ± 0.5 km s^{-1}. The masses of the hot component and the M-type giant are estimated to be 0.32 ± 0.02 $M_\odot$ and 4.6 ± 0.2 $M_\odot$, respectively, where a circular orbit with a period of 756 days is adopted. If the inner binary system has an elliptical orbit, e = 0.33, and a period of 750.1 days, the masses of the two components are 0.21 ± 0.01 $M_\odot$ and 2.2 ± 0.1 $M_\odot$, respectively. Our results lend support to the triple system model, because if the period of the symbiotic binary were 15 years, the mass of the hot component would be expected to exceed the Chandrasekhar limit. Highly blueshifted absorption components of H I and He I lines appeared at a later phase of the active stage. Mass ejections with velocities on the order of 1000 km s^{-1} seem to have occurred along the orbital plane from December 1998 to March 1999. The highest outflow velocity, –2383 km s^{-1}, was observed on 1999 February 26. Narrow absorption components of Na I D1, D2, and Fe II lines redshifted by 10−15 km s^{-1} coexisted with the highly blueshifted broad absorption components of H I and He I lines. This phenomenon might have been related to an inner disc inflow expected in wind-compressed discs. In contrast to the bipolar mass outflows at the past active stages, high-velocity equatorial mass ejections likely occurred at the active stage during the years 1998–2000. There should have been an eclipse of the hot component by the M-type giant in the inner binary system in the time period of December 1998 to January 1999. A clear light curve of the eclipse, however, was not detected. Possibly, the luminosity of the hot component was due mainly to free–free emission from the ejected circumstellar matter which was likely more extended than the M-type giant. On the other hand, another eclipse by the third component with the period of 15 years began at the end of May 1999 during which the hot component as well as the emitting regions of Hβ and Fe II lines were well eclipsed. The obscuring matter around the third component should have been much more extended than the M-type giant, and it was likely semi-transparent, because the spectrum of the M-type giant was well seen during the eclipse. The third component appears to be similar to the invisible secondary component in the long-period eclipsing binary ϵ Aur.

Key words. binaries: symbiotic – binaries: spectroscopic – binaries: eclipsing – stars: individual: CH Cyg

1. Introduction

The star CH Cyg (HD182917) was known as a normal M-type giant (M6–7 III) until Deutsch (1964) found strong blue continuum and prominent emission lines of H I, Fe II, and [Fe II] in 1963. Historical light curves are presented in previous works (e.g. Mikolajewski et al. 1990; Eyres et al. 2002; Skopal et al. 2002; Burmeister & Leedjärv 2009). There were several active stages during the years 1977–1985, 1992–1995, and 1998–2000 (e.g. Skopal et al. 2002), where the luminosity increased and emission lines of H I, He I, Fe II, [Fe II], [O III], [Ne III], [S II], and so on developed (e.g. Mikolajewski et al. 1990; Skopal et al. 1996a). Taylor et al. (1986) analysed radio images of the nebulosity around CH Cyg and found that a mass ejection with a velocity on the order of 1000 km s^{-1} had occurred at the active stage in 1984. Their result was confirmed and further mass ejections were observed during following studies (Solf 1987;

⋆ The spectra and velocities are only available at the CDS via anonymous ftp to cdsarc.u-strasbg.fr (130.79.128.5) or via http://cdsarc.u-strasbg.fr/viz-bin/qcat?J/A+A/622/A45.

Corradi et al. 2001; Crocker et al. 2001; Eyres et al. 2002; Karovska et al. 2010). Highly blue- or redshifted emission components of H I lines were found on the spectra at the active stages (Iijima et al. 1994; Skopal et al. 1996a; Tomov et al. 1996). Flickering activity was reported at the active stages (e.g. Tomov et al. 1996; Sokoloski & Kenyon 2003).

Yamashita & Maehara (1979) found a periodic variation by 15 years in radial velocities of absorption lines of the M-type giant. This period was confirmed in following publications (e.g. Tomov et al. 1996; Sokoloski & Kenyon 2003). Hinkle et al. (1993) measured radial velocities of absorption lines of the M-type giant in the infrared region and found that another periodic variation by about 750 days was superimposed on the period of 15 years. They proposed a triple system model consisting of a symbiotic binary system with an orbital period of about 750 days and third component, probably G-type dwarf, with an orbital period of 15 years. Hinkle et al. (2009), however, proposed another model with additional observations, where the orbital period of the symbiotic binary system was 15 years and the period of about 750 days was due to a pulsation of the M-type giant.

We report spectroscopic phenomena observed in the time period from October 1995 to March 2000 which covers the active stage during the years 1998–2000. Two additional spectra obtained in 2004 are presented in Sect. 4 (Fig. 13).

2. Observations

Low-resolution spectra, $\lambda/\Delta\lambda \cong 1000$ with a 600 groove mm^{-1} grating, were obtained with a Boller & Chivens spectrograph which was mounted on the 182 cm Copernics telescope at the Mount Ekar station of the Astronomical Observatory of Padova until 1997 and now is mounted on the 122 cm telescope at the Asiago Astrophysical Observatory of the University of Padova since 1998. Some low-resolution spectra in the years 1995–1997 and early 1998 were obtained with a prismatic spectrograph Camera VI mounted on the 122 cm telescope. The spectral resolution was about $\lambda/\Delta\lambda \cong 1000$ at Hβ. High-resolution spectra, $\lambda/\Delta\lambda \cong 15\,000$, were obtained with a Reosc Echelle spectrograph mounted on the 182 cm telescope. The spectra were reduced using the standard tasks of the NOAO IRAF[1] package at the Asiago Astrophysical Observatory. Spectrophotometric calibrations were performed using spectra of the standard stars HD192281 or BD+40°4032 obtained during the same nights of the observations. A log of the observations is given in Table A.1, where the phase depends on the ephemeris of Hinkle et al. (1993) for the period of 756 days: the short-period circular fit to combined data in their Table 2. Hinkle et al. (1993) chose the time of maximum positive radial velocity of the absorption lines as phase zero. We choose in this paper, however, the time of a conjunction when the hot component passed behind the M-type giant as phase zero:

$$\mathrm{JD_{conj.}} = 2446643.66 + 756.0^{d} * E. \quad (1)$$

We compare our observed results also with the ephemeris for an elliptical orbit (Hinkle et al. 2009):

$$\mathrm{JD_{conj.}} = 2447344.9 + 750.1^{d} * E, \quad (2)$$

where $e = 0.33$ and the phase zero is shifted to a conjunction.

[1] IRAF is distributed by NOAO for Research in Astronomy, Inc. under cooperative agreement with the National Science Foundation.

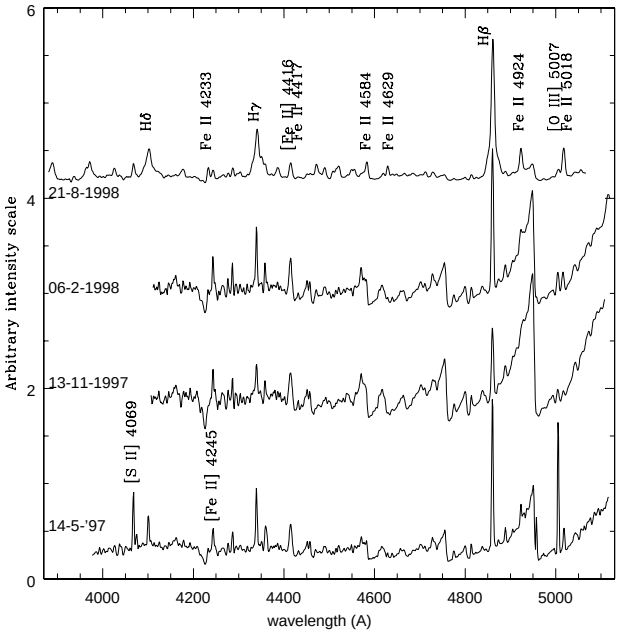

Fig. 1. Tracings of selected spectra of CH Cyg obtained at pre-active and early active stages.

3. Spectral variations

3.1. Pre-active stage and early phase of active stage

3.1.1. Low-resolution spectra

CH Cyg brightened up through May to June 1998 and entered a new active stage after the quiescent stage of about three years (e.g. Eyres et al. 2002; Burmeister & Leedjärv 2009). Figure 1 shows tracings of selected low-resolution spectra on an arbitrary intensity scale. The top tracing shows a spectrum at the active stage and the others are those at the pre-active quiescent stage. Some variations in intensity of emission lines were noticed in the quiescent stage. Their variations in intensity were not well evaluated by the equivalent widths of emission lines because the continuum level varied with the light variation of the hot component. It was also risky to compare absolute intensities of emission lines obtained with different instruments. We therefore measured intensities of emission lines relative to the depth of the TiO absorption band at 4950 Å. The intensities of the emission lines of Hβ, Fe II 5018, [Fe II] 4814, and [O III] 5007 relative to the TiO band depth are plotted in Figs. 2 and 3 on a logarithmic scale. The observational errors are about 10%. (The emission line at 5018 Å was blended with He I 5016 Å, but we write it simply as Fe II 5018 in this paper, because the line of He I was much weaker.)

As seen in Fig. 3, there was a flare-up of the emission line of [O III] 5007 in May 1997 (~JD2450580). The tracing at the bottom of Fig. 1 shows the spectrum when the emission line of [O III] 5007 had the maximum intensity which was 68% of that of Hβ. Such a high intensity was not observed even in the active stage. Karovska et al. (1998) reported that the fluxes in some bands of radio wavelength region suddenly increased in May 1997, which coincided well with the flare-up of [O III] 5007. On the other hand, the emission lines of Hβ, Fe II 5018, and [Fe II] 4814 did not show such a variation in intensity (Figs. 2 and 3). The emission line of [S II] 4069 did not show a flare-up as either. The intensity ratio [O III]/Hβ increased from 0.28 on 1997 February 10 to 0.68 on May 14, while the ratio [S II]/Hβ

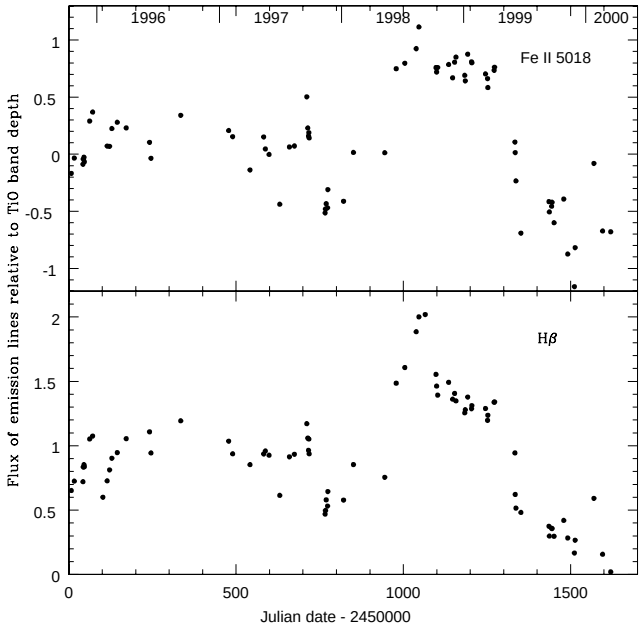

Fig. 2. Flux of emission lines of Fe II 5018 and Hβ relative to the TiO band depth on a logarithmic scale.

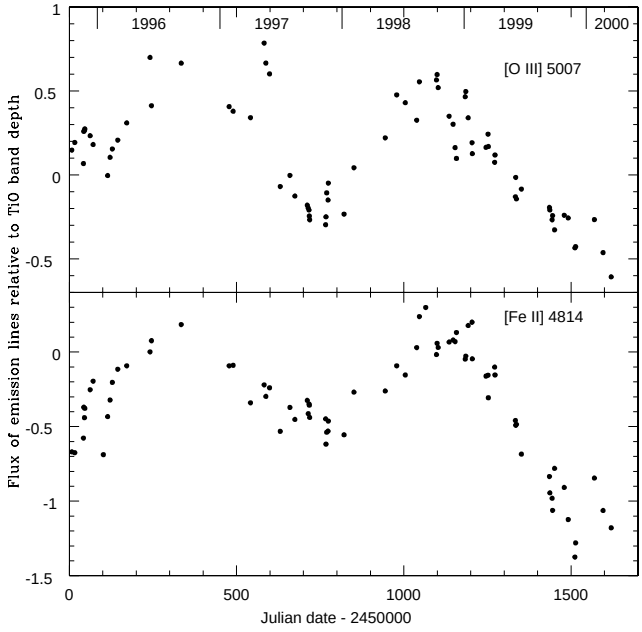

Fig. 3. Flux of emission lines of [O III] 5007 and [Fe II] 4814 relative to the TiO band depth on a logarithmic scale.

was 0.39 and 0.34 on the respective date. Any spectral feature related to the active stage, which is reported in Sect. 3.2, was not observed at that time. The emission line of [O III] 5007 subsequently faded within one month (Fig. 3), while the high level of the radio fluxes lasted one month in 8 GHz and three months in 22 GHz (Karovska et al. 1998).

All emission lines weakened around November 1997 (~JD2450770). The second tracing from the bottom in Fig. 1 shows the spectrum on which most emission lines had their local minimum intensities. The emission lines of Hβ and Fe II 5018 largely weakened between 1997 September 26 (JD2450718) and November 13 (JD2450766) as seen in Fig. 2, while the emission lines of [Fe II] 4814 and [O III] 5007 did not show such a rapid variation in intensity (Fig. 3). Burmeister & Leedjärv (2009) found a very weak emission line of Hα on 1997 October 17, which is consistent with our results. These minima of the emission lines in intensity were not related to any of the eclipses in the ephemeris of Hinkle et al. (1993, 2009). At the present time the causes of these spectral phenomena in the pre-active stage remain unknown.

The top tracing in Fig. 1 shows a spectrum at the active stage. The intensities of the emission lines of Hβ and Fe II 5018 suddenly increased between 1998 May 10 (JD2450944) and June 14 (JD2450978) as seen in Fig. 2, which coincided with the light variations (e.g. Eyres et al. 2002; Burmeister & Leedjärv 2009). On the other hand, the intensities of the emission lines of [Fe II] 4814 and [O III] 5007 increased continuously over a time period of about 300 days (Fig. 3). There were sharp peaks in the variation in intensity of the emission lines of Hβ, Fe II 5018, and probably [Fe II] 4814 around JD2451050 (Figs. 2 and 3), while there was no such peak for [O III] 5007. Burmeister & Leedjärv (2009) measured the absolute intensities and equivalent widths of the emission lines of Hβ and [O III] 5007 in the same epoch. Our results are nearly consistent with their results for the absolute intensities. The sharp peak in the variation in intensity of Hβ and lack of such a peak in [O III] 5007 are also seen in their graphs.

3.1.2. High-resolution spectra

Figure 4 shows tracings of high-resolution spectra obtained at the pre-active stage (bottom), when the luminosity was rising (middle), and at an early phase of the active stage (top). We mainly analyse the profile of Hβ in this paper, because the emission tails of Hα were blended with the [N II] 6548 and 6584 emission lines. In any case, the profiles of Hα and Hβ were nearly the same. Burmeister & Leedjärv (2009) found a double peak profile of Hα on 1998 March 23, while our spectrum on 1998 May 10 showed a nearly single peak Hβ. Therefore, the double peak profile appeared once in March and disappeared in May, then reappeared later. The emission complex of Fe II 4923.9 and He I 4921.9 showed three peaks on June 4 (Fig. 4), among which the blueward one depended on He I 4921.9. The emission line of He I 4921.9 had faded in July 1998.

The absorption component of Fe II 4923.9 was redshifted with respect to the line centre on 1998 July 9 (Fig. 4). This profile is analysed in Sect. 4.2. Numerous absorption lines of neutral metals Fe I, Cr I, Ti I, and so on were detected on July 9. They lasted in July and August, then disappeared later as reported below.

Figure 5 shows the Hβ region of high-resolution spectra on 1998 August 9 and 12 when CH Cyg was already in the active stage with $m_U \sim 8$ mag (e.g. Sokoloski & Kenyon 2003; Burmeister & Leedjärv 2009). Nearly symmetric very broad emission tails appeared on Hβ. Their full width at zero intensity (FWZI) was about 3000 km s^{-1} on August 9 and 3500 km s^{-1} on August 12.

The narrow absorption lines of the neutral metals, first detected on July 9 (Fig. 4), were quite different from those of the M-type giant. They are typically found on the spectrum of early A-type dwarfs. A tracing of HR4963 (A1 IV) is shown at the bottom of Fig. 5 as an example. We refer to these absorption lines as A-type dwarf absorption lines (AVab) hereafter. AVab are seen on the spectra of α Lyr (A0 Va), HD60778 (AO III/IV), HD85986 (A1 V), and HD161817 (sdA2), but are not seen on HR1544 (A0.5 IVn) and HR5511 (A0 V). Figure 6

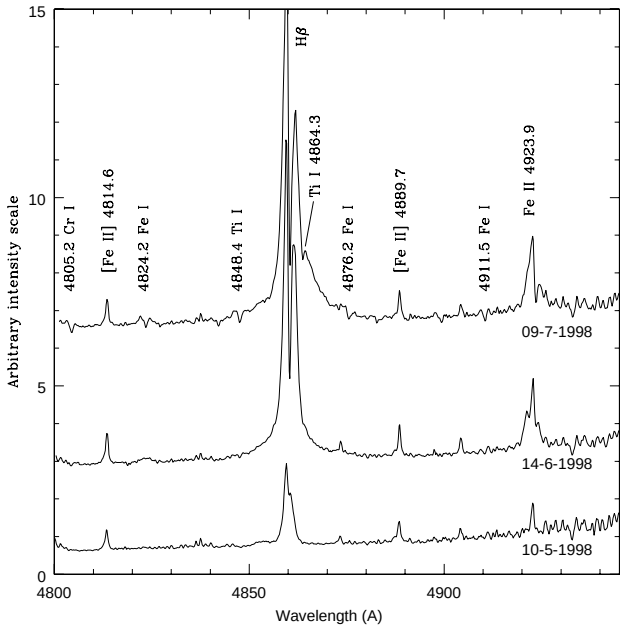

Fig. 4. High-resolution spectra of Hβ region from May to July 1998.

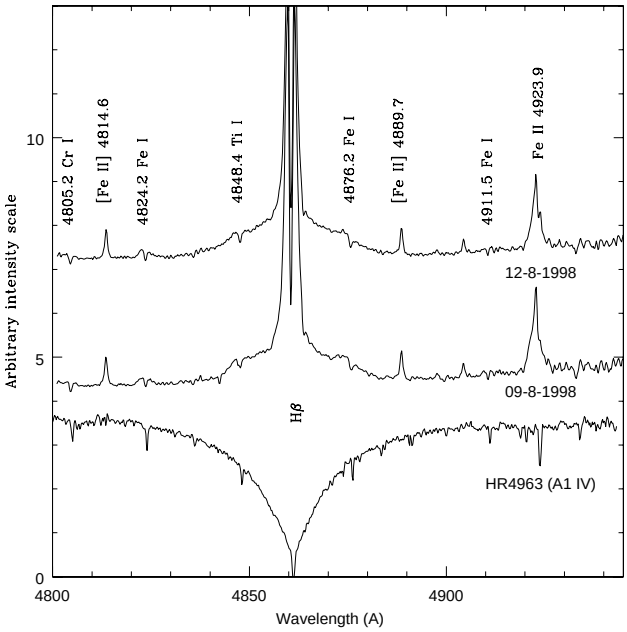

Fig. 5. High-resolution spectra of Hβ region on 1998 August 9 and 12 and a spectrum of HR4963 (A1 IV).

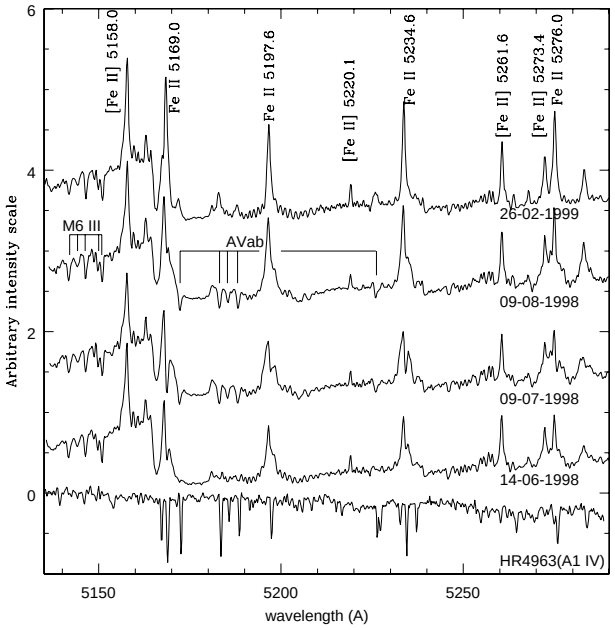

Fig. 6. High-resolution spectra in the range from 5135 Å to 5290 Å obtained from 1998 June 14 to 1999 February 26, and a tracing of HR4963 (A1 IV) is shown at the bottom.

Table 1. Parameters of the A-type dwarf absorption lines (AVab) on 1998 July 9 (JD2451004.5).

(λ_{obs}) Å	Eq.w Å	(λ_0) Å	h.r.v. km s^{-1}	Identification
4779.30	0.20	4779.89	−36.9	Cr I 124, 4779.9
4804.48	0.28	4804.92	−27.4	Cr I 283, 4805.2
4823.53	0.16	4824.13	−37.6	Fe I 888, 4824.2
4847.62	0.27	4848.22	−36.8	Ti I 217, 4848.4
4875.6:	0.11:	4876.34		Fe I 632, 4876.2
4910.53	0.12	4911.03	−30.5	Fe I 1098, 4911.5
5172.16	0.24	5172.68	−30.3	Mg I 2, 5172.7
5183.05	0.32	5183.58	−30.7	Mg I 2, 5183.6
5185.34	0.19	5185.87	−30.7	Ti I 183, 5186.3
5188.16	0.32	5188.65	−28.5	Ca I 49, 5188.9
5226.0:	0.14:	5226.42		Cr I 193, 5226.9

Notes. h.r.v.: heliocentric radial velocity.

shows tracings of selected high-resolution spectra of a different spectral region, where the absorption lines of the M-type giant and AVab are clearly visible. A tracing of HR4963 (A1 IV) is shown at the bottom of the figure. The absorption lines of the M-type giant were always seen, while the AVab appeared only in July and August 1998. Table 1 gives parameters of the AVab on 1998 July 9: those are observed wavelengths (λ_{obs}), equivalent widths, expected laboratory wavelengths of the line centre (λ_0), heliocentric radial velocities, and identifications. The values with lower accuracy are denoted by a colon. The expected laboratory wavelengths of the line centre are slightly different from those of the identified lines in the table of Moore (1959) because of blending with nearby weak lines. The lines of Cr I 5226.9 and sometimes also Fe I 4876.2 were not used to estimate the radial velocities, because the blending effects were large.

The mean of the full width at half depths (FWHD) of the AVab in July and August 1998 was about 0.55 Å, while that of HR4963 was 0.33 Å which was comparable to the resolution limit of our spectrograph. AVab of α Lyr had a mean width of about 0.6 Å. We do not know at the present time where and how the AVab in CH Cyg were formed. A physical condition similar to that of the surface of A-type dwarfs may have happened in a part of the system of CH Cyg. As shown in Sect. 4.1, the AVab were redshifted by about 30 km s^{-1} with respect to the absorption lines of the M-type giant. The AVab was therefore unlikely to be related to a mass outflow even though they appeared in the active stage. Such a physical condition may also be unlikely to have happened around the M-type giant or in the wind-colliding region (Contini et al. 2009a,b). We estimate that the AVab were

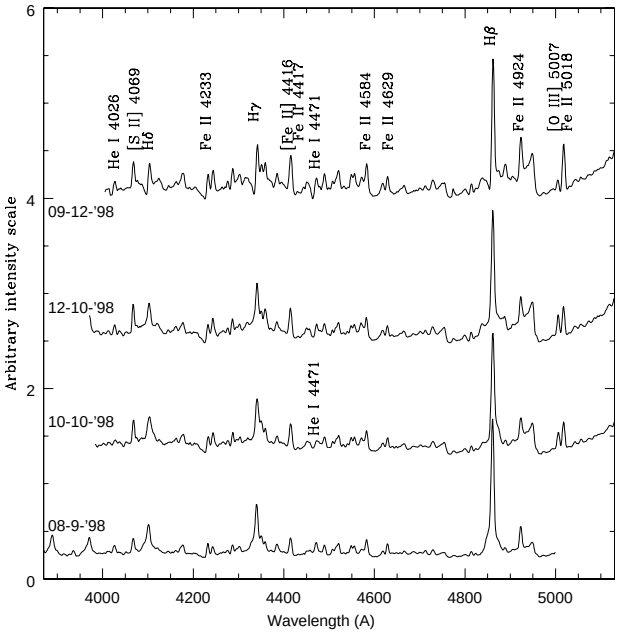

Fig. 7. Low-resolution spectra obtained from 1998 September 8 to December 9.

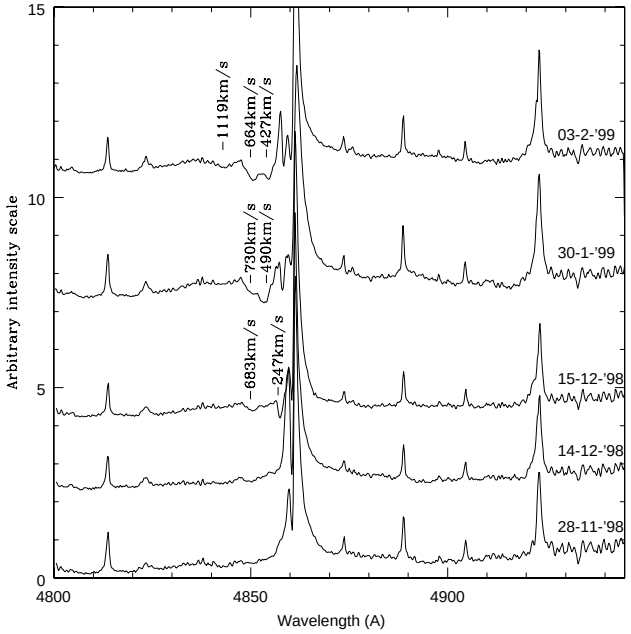

Fig. 8. High-resolution spectra obtained from 1998 November 28 to 1999 February 3.

formed on the surface of the pseudo-photosphere around the hot component at an early phase of the active stage. We also estimate that their redshifts were due to the orbital motion of the hot component. Detailed analyses for the radial velocities of the AVab are made in Sect. 4.1.

AVab are not rare among the spectra of symbiotic stars in active stage. We found them at least on BF Cyg in March 2016, BX Mon in January 2017, and RS Oph in April 2018. These results will be presented in forth coming papers.

Some AVab appeared as emissions at a later phase of the active stage as seen on the top tracing in Fig. 6.

3.2. Outflow phase of active stage

3.2.1. Low-resolution spectra

Figure 7 shows tracings of selected low-resolution spectra from September to December 1998. The spectrum on September 8 was nearly the same as that on August 21 (Fig. 1). The spectral features changed between September 8 and October 10, for example the profile of Hβ became asymmetric and an absorption component appeared on He I 4471. Broad emission components appeared at both sides of H I lines on October 12. Those of Hβ were extended in the range $\pm$2100 km s^{-1} at zero intensity level. P Cyg-type absorptions appeared on H I and He I lines on December 9 and the broad emission components of Hβ became still wider, $\pm$2500 km s^{-1}. The absorption component of Hβ was blueshifted by $-$490 km s^{-1} from the narrow emission component. These spectral features suggested that a strong mass ejection occurred during this epoch. Similar profiles were found by Tomov et al. (1996) in May 1994.

3.2.2. High-resolution spectra

Figure 8 shows tracings of selected high-resolution spectra from 1998 November 28 to 1999 February 3. The AVab had disappeared in November 1998. The two emission peaks of Hβ had comparable heights in August 1998 (Fig. 5), while the blueward peak was significantly lower than the redward one in November 1998 and later. The blueward peak was probably whittled down by blueshifted broad absorption components. The asymmetric profile of Hβ on the low-resolution spectrum on 1998 October 10 (Fig. 7) may have been due to the fading of the blueward peak.

The blueshifted broad absorption component appeared clearly in December 1998. A rather narrow, deep absorption component and a broad, shallow absorption component appeared on December 15 which were not seen one day before (Fig. 8). The heliocentric radial velocities of the former was $-$247 km s^{-1} and that of the bottom of the broad absorption component was $-$683 km s^{-1}. The broad absorption component had by then become deeper in January 1999 and later. The broad absorption component on January 30 seems to have consisted of two parts with radial velocities of $-$490 km s^{-1} and $-$730 km s^{-1}. This profile is similar to those observed by Tomov et al. (1996) in 1994. They found a broad absorption component of Hβ consisting of two parts, the radial velocities of which were about $-$500 km s^{-1} and $-$700 km s^{-1}. The part with the radial velocity of $-$500 km s^{-1} was significantly deeper than the other one in 1994 (Tomov et al. 1996). In our case, however, the part with the higher negative velocity was slightly deeper on February 3 (Fig. 8). There was one more broad and shallow absorption component with radial velocity of $-$1119 km s^{-1} and FWHD 200 km s^{-1}. The emission tails of Hβ in these dates extended more than $\pm$2000 km s^{-1}, but it was difficult to determine the precise limits.

Figure 9 shows tracings of selected high-resolution spectra in February and March 1999. The broad absorption component had a nearly flat bottom on February 13. The heliocentric radial velocity of the middle of the absorption trough was $-$620 km s^{-1} and FWHD was 360 km s^{-1}. There was probably one more very shallow absorption component with a flat bottom extended from 4841 Å ($-$1272 km s^{-1}) to 4847 Å ($-$870 km s^{-1}). The emission tails of Hβ seems to have shrunk to $\pm$1500 km s^{-1}.

A mysterious spectral feature, which never before been reported, appeared on 1999 February 26 (Fig. 9). There were three absorption components with radial velocities of $-$2464 km s^{-1}, $-$1714 km s^{-1}, and $-$691 km s^{-1}, as indicated on

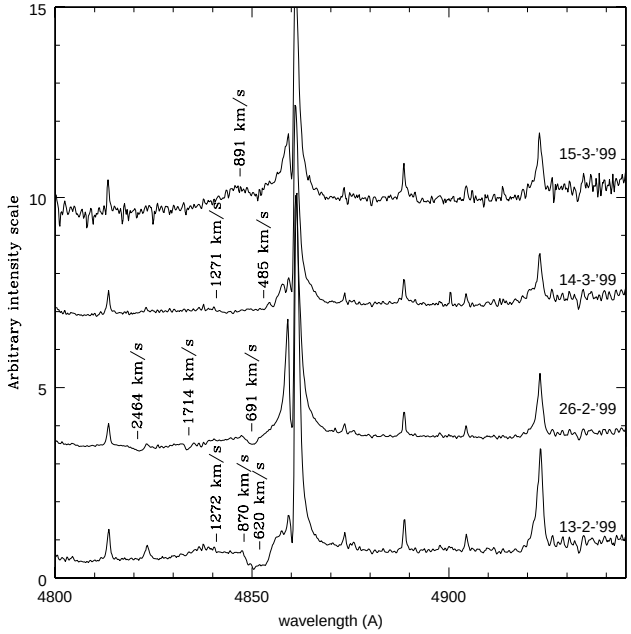

Fig. 9. High-resolution spectra obtained from 1999 February 12 to March 15.

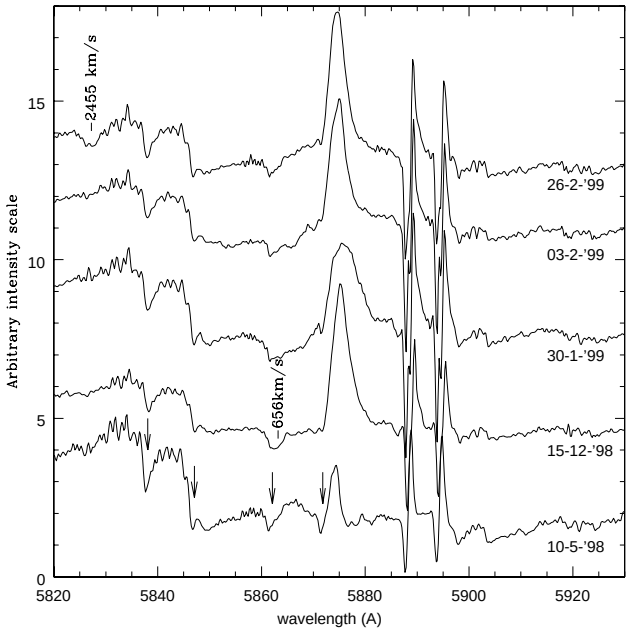

Fig. 10. High-resolution spectra around He I 5876 from 1998 May 10 to 1999 February 26. The absorptions indicated by an arrow depended on the M-type giant.

the tracing. The heliocentric radial velocity of the hot component in the binary system was expected to have been −81.2 km s^{-1} at that time (see Sect. 4.1). The maximum outflow velocity was therefore −2383 km s^{-1}. We would like to call the attention of the reader to the extremely high velocity outflow occurring along the line of sight, namely along the orbital plane, because CH Cyg is an eclipsing binary.

A very shallow absorption component with a flat bottom was seen on March 14. It was extended in the range from 4841 Å (−1271 km s^{-1}) to 4857 Å (−485 km s^{-1}). The broad absorption component disappeared one day later and a broad emission component appeared (Fig. 9). The radial velocity of its peak was −891 km s^{-1} and the FWHM was 470 km s^{-1}. No broad absorption component was detected after that time. The large mass ejection seems to have terminated around the middle of March 1999.

The rather narrow absorption component, *FWHD* ∼ 70 km s^{-1}, was deeper than the broad one on 1998 December 15, then decreased in depth with time (Fig. 8). It was very weak on 1999 February 13 and disappeared on February 26, then reappeared on March 14 (Fig. 9). Its radial velocity changed from −247 km s^{-1} on 1998 December 15 to −165 km s^{-1} on 1999 March 14 almost linearly with time.

3.2.3. Emission and absorption components of He I 5876

Figure 10 shows tracings of selected high-resolution spectra of the He I 5876 region. A spectrum at the quiescent stage on 1998 May 10 is shown at the bottom of the figure, where the absorption bands indicated by an arrow at 5838 Å, 5847 Å, 5862 Å, and 5872 Å depended on the M-type giant. These are complexes of the TiO molecular bands and absorption lines of Fe I, Cr I, and so on. The absorption at 5865 Å on 1998 December 15 was certainly an absorption component of He I 5876 blueshifted by −656 km s^{-1} because it was significantly deeper than the absorption band of the M-type giant. The absorption at about 5830 Å on 1999 February 26 was also the absorption component of He I 5876 with a radial velocity of −2455 km s^{-1}, because there was no absorption band of the M-type giant at that position. On the other hand, it was difficult to see the profiles of the broad absorption components on the other spectra. In order to make the profiles more visible, the spectrum of the quiescent stage was subtracted from those at the active stage. The results are shown in Figs. 11 and 12.

The profiles of the broad absorption components of He I 5876 were almost similar to those of Hβ from 1998 December 15 to 1999 February 13 (Figs. 8, 9 and 11). A large difference was found on 1999 February 26, when Hβ had three absorption components, while only that of the highest blueshift was clearly seen for He I 5876 (Fig. 12). The corresponding positions for the absorption components of Hβ with the lower blueshifts are indicated by an arrow. The broad absorption component of Hβ was very shallow on 1999 March 14 (Fig. 9), while He I 5876 had two absorption components with heliocentric radial velocities of −562 km s^{-1} and −979 km s^{-1} (Fig. 12). The profile of the broad absorption component of He I 5876 changed one day later. In contrast to Hβ, which had a broad emission component, a weak absorption with a nearly flat bottom was seen on 1999 March 15 (Fig. 12). The heliocentric radial velocity of the middle of the absorption trough was −458 km s^{-1} and FWHD was 517 km s^{-1}.

The emission component of He I 5876 was thick on 1999 January 30 (Fig. 10). The emission components of Hβ and Fe II 4921.9 on the same spectrum did not show such a profile (Fig. 8), nor did the emission component of He I 5876 on any of our other spectra at the active stage. The cause of the thickness is not known.

3.3. Final phase of the active stage

An eclipse with the period of 15 years (Hinkle et al. 2009) began at the end of May 1999 (∼JD2451330) and the low level in U mag lasted about 180 days (Eyres et al. 2002; Burmeister & Leedjärv 2009). The luminosity in U band

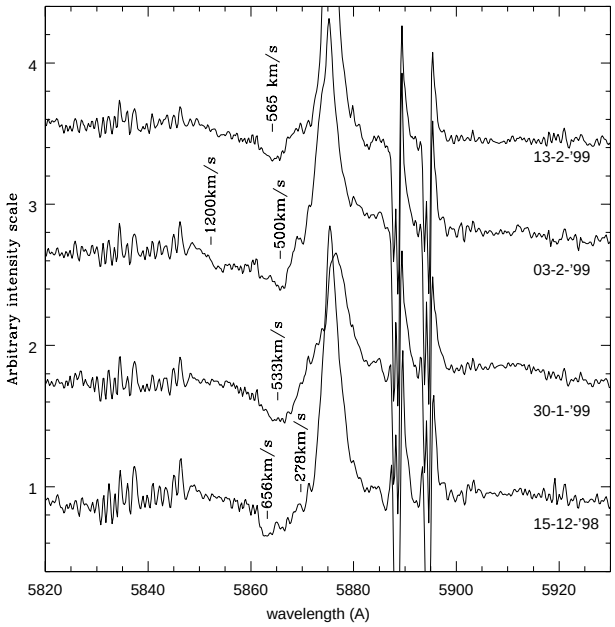

Fig. 11. High-resolution spectra around He I 5987 from 1998 December 15 to 1999 February 13 after the subtraction of the quiescent spectrum.

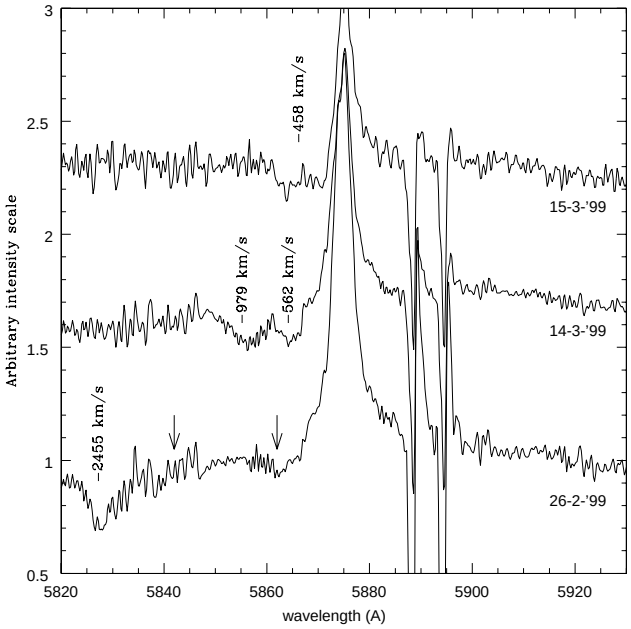

Fig. 12. High-resolution spectra around He I 5987 from 1999 February 26 to March 15 after the subtraction of the quiescent spectrum. Arrows indicate the corresponding positions of the absorption components of Hβ with the lower blueshifts.

slightly recovered at the end of the eclipse in January 2000 (~JD2451550) by $\Delta U \sim 1$ mag (e.g. Eyres et al. 2002; Skopal et al. 2002), after which it faded slowly and CH Cyg entered a long quiescent stage (Burmeister & Leedjärv 2009; Wallerstein et al. 2010).

The intensities of the emission lines of Hβ and Fe II 5018 suddenly decreased at the end of May 1999 (Fig. 2) which closely coincided with the light variation. On the other hand, the intensities of the emission lines of [O III] 5007 and [Fe II] 4814 decreased slowly (Fig. 3). The emitting regions of the latter lines were possibly more extended and the effect of the eclipse was

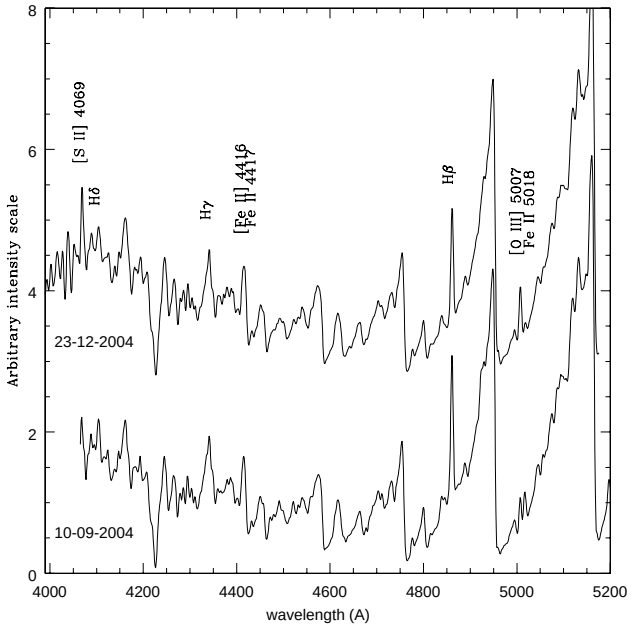

Fig. 13. Low-resolution spectra obtained on 2004 September 10 and December 23.

small. The slow fading of these emission lines may have reflected the decreasing activity of the hot component.

When the eclipse passed in January 2000, the emission lines of Hβ and Fe II 5018 recovered their intensities (Fig. 2) a little. The intensities of the lines of [O III] 5007 and [Fe II] 4814 also recovered a little at the same time (Fig. 3). The emitting regions of the latter lines had probably shrunk owing to the decrease in the activity of the hot component, and therefore the effects of the eclipse were not negligible at that time.

4. Radial velocities of absorption and emission lines and an argument against the long-period binary model

Munari et al. (1996) criticised the triple system model for CH Cyg by Hinkle et al. (1993). Their argument, however, was based on some arbitrary hypotheses: for example, white dwarfs with a mass of 0.2 $M_\odot$ are quite unusual, or the mass of the M-type giant should have been about 1.0 $M_\odot$. Evidence contradicting these lines of argument has since been found and therefore their criticisms are no longer valid.

Balega et al. (2007) performed interferometric observations in October 2004 and found a faint object of 43 or 41 milliarcseconds (mas) detached from the M-type giant. Detailed analyses of their images were made by Mikolajewska et al. (2010) who concluded that the faint object was the hot component on the outer orbit with the period of 15 years. Such an object, however, was not confirmed by the infrared interferometry performed by Pedretti et al. (2009) in the same year.

Figure 13 shows tracings of low-resolution spectra obtained on 2004 September 10 and December 23 in our observatory. As seen in the figure all emission lines were weak. The equivalent widths of Hβ and [O III] 5007 were −8.2 Å and −1.8 Å on September 10 and −10.1 Å and −5.4 Å on December 23. These values were comparable to those on 1997 November 13 (Fig. 1) when all emission lines had their local minimum intensities. The

equivalent widths of Hβ and [O III] 5007 were −10.8 Å and −2.3 Å at that date.

Mikolajewska et al. (2010) estimated the luminosity of the faint object to have been about 2 mag fainter than the M-type giant in the optical region. They claimed that CH Cyg was in a mild active stage because the emission lines of H I, Fe II, and [O III] were detected (Yoo 2007), and therefore the hot component had a high luminosity in the optical region. Yoo (2007), however, did not measure the intensities or equivalent widths of the emission lines. The weakness of the emission lines (Fig. 13) suggests low activity of the hot component in the latter half of 2004. Contini et al. (2009a) also suggested low activity of the hot component in 2004. It is unlikely that the hot component had a luminosity only 2 mag fainter than the M-type giant in such a low stage. The images of the faint object obtained by Balega et al. (2007) might have been related to the equatorial mass ejection in 1999 (Sect. 3.2), unless they were due to ghosts or something else.

Pedretti et al. (2009) performed infrared interferometry towards CH Cyg and found an asymmetry in the image of the M-type giant which moved according to the period of about 750 days. Their result supports the model of the inner symbiotic binary, that is, the triple system for CH Cyg. Our observed results are compared with their work in Sect. 4.3.

We first analyse in this section our spectroscopic data adopting the circular orbit model for the inner binary (Hinkle et al. 1993), and then an argument for the elliptical orbit (Hinkle et al. 2009) is made in Sect. 4.3.

4.1. Orbital elements of the binary system

Radial velocities of the absorption lines of the M-type giant and the AVab were measured. We selected 15 absorption lines of the M-type giant in the spectral region from 5120 Å to 5440 Å. Some AVab appeared as emission at the later phase of the active stage and their radial velocities were also measured. The mean radial velocities and errors are given in Table 2, where radial velocities with the superscript *a* are those of AVab in emission. The phase in the table depends on the ephemeris for the circular orbit (Eq. (1)). The results are plotted in Fig. 14, where dots are the radial velocities of the absorption lines of the M-type giant, solid circles are AVab, and crosses are AVab in emission. Triangles are radial velocities of the absorption lines of the M-type giant in the infrared region measured by Hinkle et al. (2009). The absorption lines of the M-type giant in our optical region were slightly redshifted with respect to the infrared ones. We are afraid that the irradiation of the M-type giant by the hot component produced some changes in the profiles of the absorption lines in the optical region. Therefore, the radial velocities of the absorption lines in the infrared region (Hinkle et al. 2009) are used in the following analyses.

The radial velocities of the AVab were significantly detached from those of the absorption lines of the M-type giant (Table 2 and Fig. 14). If the radial velocities of the AVab represent the orbital motion of the hot component, our results lend support to the triple system model proposed by Hinkle et al. (1993), where the orbital period of the symbiotic pair was about 750 days. If the orbital period of the symbiotic pair were about 15 years, the mass of the hot component would likely exceed the Chandrasekhar limit.

Unfortunately, the AVab were detected only in July and August 1998, that is, phase 0.71 to 0.81 in the period of 756 days. We examined other elements to see whether their radial velocities represented the orbital motion of the hot component. Some AVab appeared as emission at the later phase of the active stage, but their radial velocities were roughly stable with time (Table 2 and Fig. 14). The emission line of He I 5876 showed a double peak profile in June 1999 and later. Sometimes the radial velocity of one of the peaks agreed with the expected radial velocity of the hot component, but not always. Figure 15 shows the profiles of the emission components of He I 5876. The peaks indicated by an arrow had radial velocities in agreement with the orbital motion of the hot component. We were, however, unable to distinguish which peak was that of the hot component without prior knowledge of its orbital motion, and so we did not adopt the peak of the emission line of He I 5876 as an indicator of the orbital motion of the hot component.

The radial velocities of the absorption and emission lines are plotted against the phase of the period of 756 days in Fig. 16.

Table 2. Radial velocities in km s^{-1} of absorption lines of the M-type giant and those of the A-type dwarfs (AVab).

Date	JD	Phase	M giant		AVab	
yy/mm/dd			R.V.	error	R.V.	error
96/09/07	334.5	0.882	−64.7	1.1		
97/01/29	477.7	0.071	−61.2	0.8		
97/01/30	478.7	0.073	−59.2	0.8		
97/02/21	500.7	0.102	−61.8	0.8		
97/03/29	536.6	0.149	−60.1	0.8		
97/03/31	538.6	0.152	−62.4	0.8		
9704/01	539.6	0.153	−59.0	0.8		
97/05/30	598.6	0.231	−60.8	0.8		
97/07/01	630.6	0.274	−61.5	0.9		
98/05/10	944.5	0.689	−65.4	1.0		
98/06/14	978.6	0.734	−65.2	1.0	−28.2	3.1
98/07/09	1004.5	0.768	−63.4	1.0	−32.1	1.3
98/08/09	1035.5	0.809	−65.8	0.9	−27.6	1.0
98/08/10	1035.6	0.809	−66.9	0.7	−30.3	1.2
98/08/12	1038.5	0.813	−62.0	1.0	−30.6	1.5
98/11/28	1146.3	0.956	−60.2	1.2	−46.4^a	3.4
98/12/13	1161.3	0.976	−60.8	0.9		
98/12/14	1162.3	0.977	−59.1	0.9		
98/12/15	1163.3	0.978	−61.4	0.9	−43.9^a	3.1
99/01/30	1208.7	0.038	−62.2	0.9	−41.9^a	2.6
99/02/03	1212.7	0.044	−59.6	0.9		
99/02/13	1222.7	0.057	−56.9	1.0	−41.2^a	3.3
99/02/17	1226.7	0.062	−61.8	1.2	−42.9^a	2.3
99/02/26	1235.7	0.074	−60.7	0.9	−44.0^a	2.9
99/03/14	1251.6	0.095	−58.5	0.9	−43.2^a	4.8
99/03/15	1252.6	0.097	−59.2	1.0		
99/04/02	1270.6	0.120	−58.4	0.9		
99/04/03	1271.6	0.122	−58.0	0.8	−41.2^a	2.8
99/04/04	1272.6	0.123	−58.7	1.0	−42.0^a	4.2
99/06/04	1333.5	0.204	−59.2	0.7		
99/06/07	1336.6	0.208	−59.8	0.9		
99/09/28	1450.4	0.358	−60.3	0.8		
00/01/26	1569.7	0.516	−57.3	0.8		
00/02/21	1595.7	0.550	−58.3	0.8		
00/03/16	1619.6	0.582	−61.5	0.8		
00/04/26	1660.5	0.636	−61.4	1.0		
00/05/15	1679.6	0.661	−63.6	0.9		
00/05/16	1680.6	0.663	−65.0	1.2		

Note. JD: Julian date – 2450000. $^{(a)}$AVab in emission.

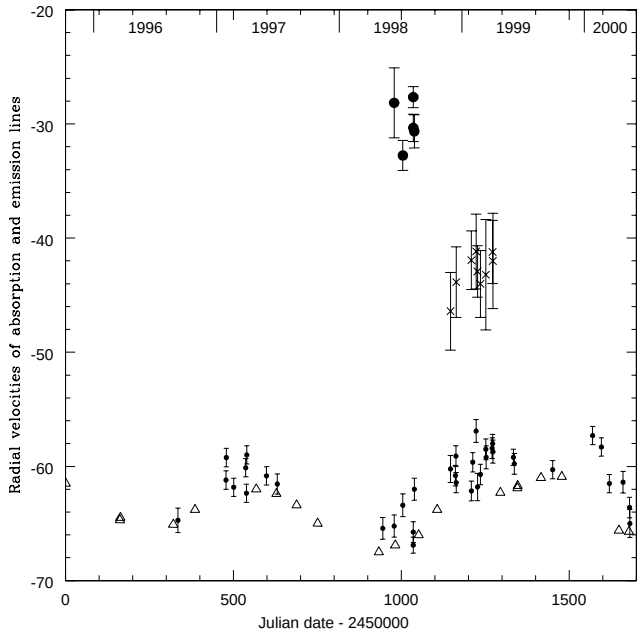

Fig. 14. Radial velocities in km s^{-1} of absorption and emission lines, where dots are the radial velocities of the absorption lines of the M-type giant, solid circles are AVab, crosses are AVab in emission, and triangles are infrared absorption lines measured by Hinkle et al. (2009).

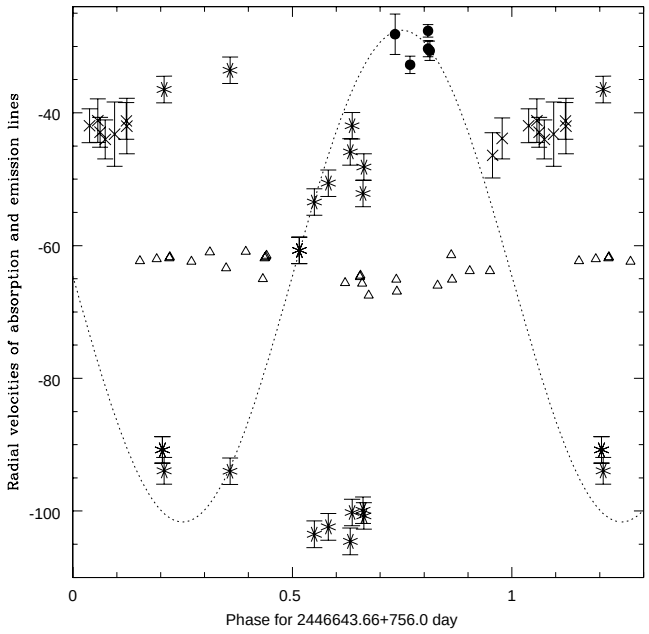

Fig. 16. Radial velocities of absorption and emission lines against the period of 756 days. Asterisks mark the two emission peaks of He I 5876 and the other symbols are the same as in Fig. 14. The dotted line exhibits the radial velocity of the hot component.

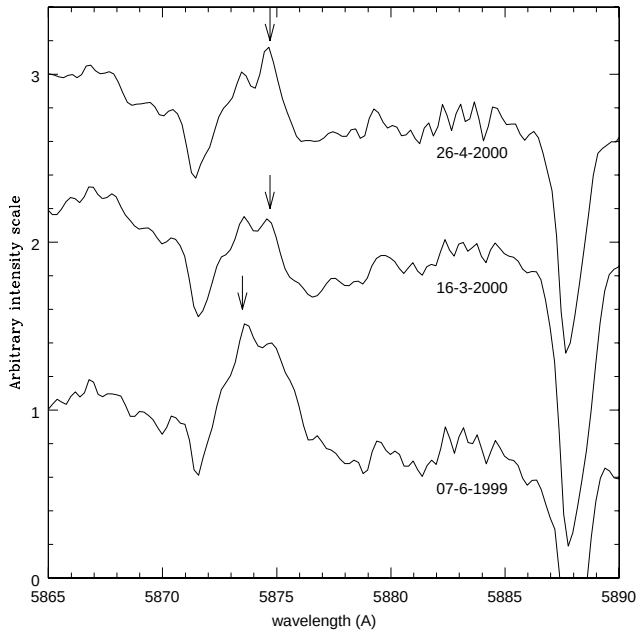

Fig. 15. Selected profiles of the emission component of He I 5876. The peaks indicated by an arrow had radial velocities in agreement with the orbital motion of the hot component.

The radial velocities of the two peaks of the emission line of He I 5876 are plotted by an asterisk and the other symbols are the same as in Fig. 14. Hinkle et al. (1993) obtained $K_2 = 2.61 \pm 0.12$ km s^{-1} for the M-type giant, and the γ velocity of the inner binary in 1998 should have been -64.6 km s^{-1}. We inferred $K_1 = 37.0 \pm 0.5$ km s^{-1} assuming $\gamma = -64.6$ km s^{-1}. The radial velocity of the hot component in 1998–1999 is expected to be:

$$v_{\rm hot} = -37.0 \times \sin[2\pi(t - t_0)/756.0] - 64.6 \text{ km s}^{-1}, \quad (3)$$

where t is Julian date and t_0 is 2450423.66. The dotted line in Fig. 16 exhibits the expected radial velocity of the hot component.

The masses of the two components are estimated to be $M_1 = 0.32 \pm 0.02\,M_\odot$ and $M_2 = 4.6 \pm 0.2\,M_\odot$ for the circular orbit (see Sect. 4.3 for the elements of the elliptical orbit). The radius of the Roche lobe for the M-type giant is 380 $R_\odot$. The M-type giant is unlikely to have filled the Roche lobe, but a part of its outer atmosphere could have expanded beyond the Roche lobe and fallen down to the hot component. The mass transfer in the binary system was likely due to this type of soft Roche lobe overflow.

Skopal et al. (1998) found that the radial velocity of UV emission lines measured by IUE varied according to the period of 756 days, but with a lower semi-amplitude of about 20 km s^{-1}. We guess that they measured the radial velocity of the line centre of the UV emission lines. It is, however, unclear whether or not the line centre of emission lines represents the orbital motion of the hot component, as seen for example in the case of He I 5876 (Figs. 15 and 16). The radial velocities of the UV emission lines may have partly represented the orbital motion of the hot component.

4.2. Redshifted absorption lines

Figure 17 shows tracings of selected spectra in the Na I D1 and D2 regions. The radial velocities of their main absorption components were nearly stable and were found in the range -109 ± 5 km s^{-1}. They were probably related to the circumstellar matter ejected during the previous active stages. Secondary absorption components appeared at the redward sides of the emission components on 1998 July 9 as indicated by arrows. Their radial velocities were about -17 km s^{-1}, that is, redshifted by 15 km s^{-1} with respect to the AVab. Absorption components with similar radial velocities were detected on the emission lines of Fe II on the same spectrum (Figs. 4 and 6). The redshifted

Table 3. Radial velocities of the main and secondary absorption components of Na I D1 and D2 and mean radial velocities of the absorption components of Fe II lines.

Date	JD	Phase	Radial vel.					
			Na I D2		Na I D1		Fe II	error
yy/mm/dd			main	sec.	main	sec.		
98/06/14	978.6	0.734					−16.5	1.4
98/07/09	1004.5	0.768	−107.9	−13.3	−105.5	−19.0	−19.4	1.8
98/08/09	1035.5	0.809	−112.4	−14.2	−108.5	−19.5		
98/08/10	1035.6	0.809	−113.7	−14.9	−110.2	−23.8		
98/08/12	1038.5	0.813	−107.3	−18.2	−105.4	−20.6	−27.3	2.0
98/12/13	1161.3	0.976	−106.0	−59.0	−106.6	−58.9		
9901/30	1208.7	0.038	−112.8	−72.2	−113.3	−71.6		
99/02/03	1212.7	0.044	−110.5	−66.8	−111.4	−65.6		
99/02/13	1222.7	0.057	−109.3	−64.6	−110.5	−63.7		
99/02/17	1226.7	0.062	−109.9	−66.1	−110.1	−65.4		
99/02/26	1235.7	0.074	−110.1	−69.9	−106.6	−70.0		
99/03/14	1251.6	0.095	−104.0	−75.2	−103.7	−71.7		

Notes. JD: Julian date – 2450000. Errors in the radial velocities of Na I lines are ±2.0 km s^{-1}.

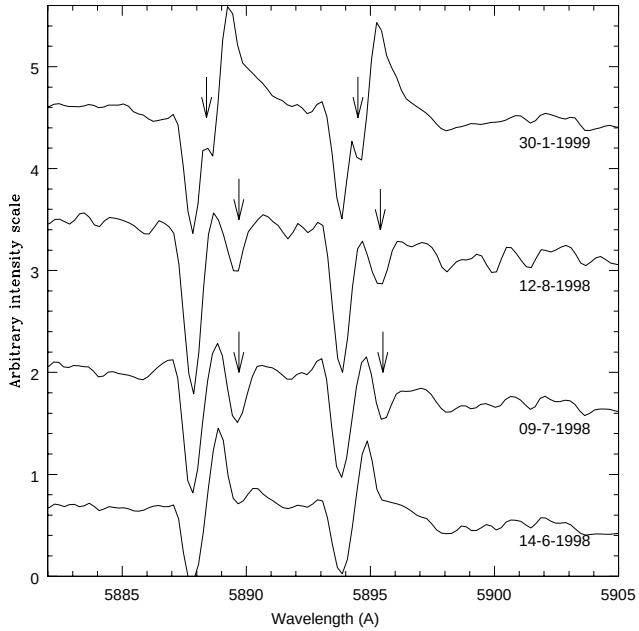

Fig. 17. Profiles of Na I D1 and D2 lines. Arrows indicate their secondary absorption components.

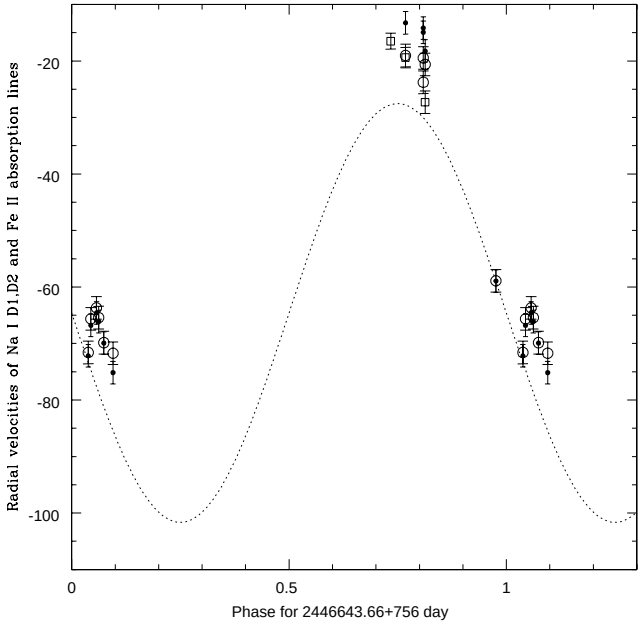

Fig. 18. Radial velocities of the absorption lines, where dots and open circles indicate the secondary absorption components of Na I D1 and D2, respectively, and squares the Fe II lines. The dotted line exhibits the radial velocity of the hot component.

absorption components of Fe II were seen on June 14 and July 9 (Figs. 4 and 6) and had faded in August (Figs. 5 and 6), while those of Na I lasted through August (Fig. 17). The secondary absorption components of Na I appeared at the blueward sides of the emission components in the epoch from December 1998 to March 1999. The profiles on 1999 January 30 are shown in Fig. 17. The radial velocities of these absorption components are given in Table 3 and are plotted against the phase of the period of 756 days in Fig. 18.

These absorption lines were possibly formed in regions close to the hot component, because their radial velocities varied following its orbital motion (Fig. 18). Meanwhile, the absorption components were generally redshifted by 10−15 km s^{-1} towards the hot component with a few exceptions. It is noteworthy that high-velocity mass ejections were observed from November 1998 through March 1999 (Sect. 3.2) which corresponds to phase 0.95 to 1.10 in Fig. 18. It seems that the redshifts of the absorption components were not affected by the mass ejections.

High-velocity mass ejections along the orbital plane, namely equatorial ejections, were rather similar to those from rapidly rotating stars such as Be stars. Owocki et al. (1994) found that high-velocity outflows and an inner disc inflow occur contemporaneously in their simulation for wind-compressed discs. The redshifted absorption components of Na I and Fe II lines might have been related to this mechanism.

Skopal et al. (2002) found absorption components redshifted by approximately 100 km s^{-1} on the higher members of H I Balmer series at the active stage in 1981. They suggested that there was a high-velocity inflow in the system of CH Cyg. Their

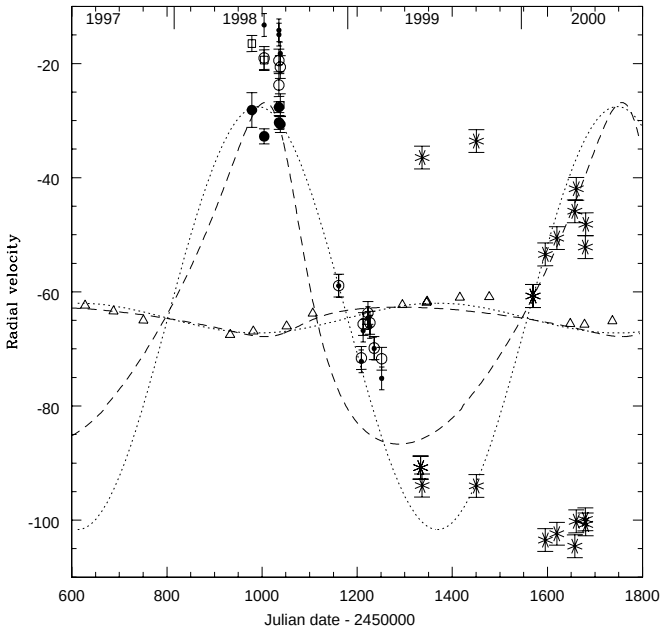

Fig. 19. Radial velocities of AVab (solid circle), two emission peaks of He I 5876 (asterisk), redshifted absorption components of Na I D1 and D2 (dot and open circle), the redshifted absorption component of Fe II lines (open square), and absorption lines in the infrared region of the M-type giant (triangle). The dotted lines exhibit the radial velocities of the hot component and the M-type giant in the circular orbit, while the broken lines indicate those in the elliptical orbit.

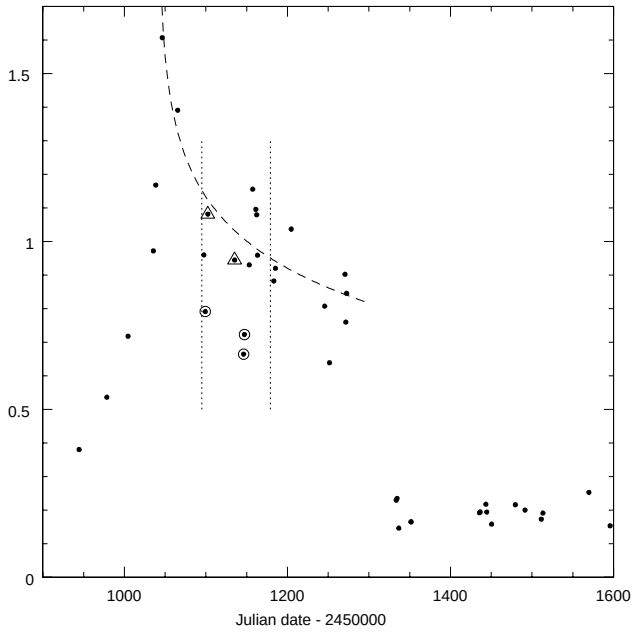

Fig. 20. Luminosity of the hot component relative to the depths of TiO absorption bands at 4755 Å and 4950 Å on a logarithmic scale. The broken line exhibits an expected light curve in the decline phase. Two vertical dotted lines indicate the expected dates of an eclipse in the elliptical orbit (JD2451095) and the circular orbit (JD2451179).

inflow was likely a different phenomenon, because our redshifts were only one tenth the size of theirs. Unfortunately a direct comparison was not possible, because our spectra did not cover the spectral region for the higher members of H I Balmer series.

4.3. Circular orbit or elliptical orbit?

Figure 19 shows radial velocities of the AVab (solid circle), two emission peaks of He I 5876 (asterisk), redshifted absorption components of Na I D1 and D2 (dot and open circle), the redshifted absorption component of Fe II lines (open square), and absorption lines of the M-type giant in the infrared region (triangle) measured by Hinkle et al. (2009). The dotted lines exhibit the radial velocities of the hot component and the M-type giant in the circular orbit with the period of 756 days (Hinkle et al. 1993) and the broken lines indicate those of the elliptical orbit with $e = 0.33$ and the period of 750.1 days (Hinkle et al. 2009). The semi-amplitudes of the orbital motions of the hot component are chosen to fit well the radial velocities of the AVab.

The radial velocities of the redshifted absorption components of Na I and Fe II lines and one of the two emission peaks of He I 5876 on some dates appear to agree with the circular orbital motion. On the other hand, the radial velocities of an emission peak of He I 5876 agree more closely with that of the elliptical orbit from JD2451570 to 2451660. In the previous sections, we analysed the spectroscopic data assuming the circular orbit. The elliptical orbit, however, could not be rejected with our present data. The semi-amplitude of the radial-velocity variation of the hot component in the elliptical orbit is $K_1 = 30.0 \pm 0.5$ km s^{-1}. The masses of the two components are $M_1 = 0.21 \pm 0.01\ M_\odot$ and $M_2 = 2.2 \pm 0.1\ M_\odot$ where the period is 750.1 days and $K_2 = 2.87 \pm 0.13$ km s^{-1} (Hinkle et al. 2009). The radius of the Roche lobe is about 270 $R_\odot$.

In the case of the circular orbit (Sect. 4.1), our spectroscopic results give a diameter of about 600 $R_\odot$ for the orbit of the hot component which corresponds to 11.5 mas at a distance of 244 pc to CH Cyg (van Leeuwen 2007). The separation between the M-type giant and the hot component may be about 6 mas. Pedretti et al. (2009) estimated the separation between the M-type giant and the faint companion to have been 6–8 mas by their infrared interferometric observations which is consistent with our result.

In the case of the elliptical orbit, our results give a separation of about 5 mas. It would perhaps be hasty, however, to conclude with these results that the circular orbit better agrees with the observed phenomena, because our argument is based on the radial velocities of AVab in the restricted epoch.

Pedretti et al. (2009) estimated the positions of the companion relative to the M-type giant with the interferometry. They showed that the companion was moving towards the point of conjunction in front of the M-type giant in August and September 1999 (~JD2451430). Their results agree with the expected orbital motions of the hot component both in the circular and elliptical orbits (Fig. 19).

5. The third component in the triple system

We estimated the luminosity of the hot component relative to the depth of TiO absorption bands. To do this, we measured the heights of the head (a) and bottom (b) of the band; the depth of the absorption band is $(a - b)$. The ratio $a/(a - b)$ could exhibit the flux of the underlying continuum relative to the depth of the absorption band. We did not use the ratio $b/(a - b)$ because of larger observational errors. The TiO absorption bands at 4755 Å and 4950 Å are used and the mean of the ratios of the two bands are plotted in Fig. 20 on a logarithmic scale: $2.5 \log(a/(a - b))$.

The brightening up of the hot component in the epoch from JD2450900 to 2451040 is well followed with this quantity

(Fig. 20). The broken line exhibits an expected light curve of the hot component in the decline phase: $-0.5\ \log(t - t_0) + 2.05$, where t is the Julian date and t_0 is 2451042.

The circular orbit should have led to an eclipse of the hot component by the M-type giant on JD2451179 (Eq. (1)), whereas the elliptical orbit should have led to this happening on JD2451095 (Eq. (2)). These dates are indicated by vertical dotted lines in Fig. 20. The errors in the dates of the eclipse are about ±20 days (Hinkle et al. 1993, 2009). The low luminosities of the hot component presented by a dot in a circle might have been related to the eclipse. A clear light curve of the eclipse was not seen however, because the luminosities presented by a dot in a triangle, were not particularly faint even when the eclipse was supposed to be ongoing.

Skopal et al. (1996b) found fading of the luminosity of CH Cyg in the U band with a period of 756 days in the years from 1968 to 1973, but such periodic fading was not seen during the active stage from 1978 to 1985 (Skopal et al. 1996b). Iijima (1998) found a clear light curve of an eclipse in 1994 using the depth of the TiO absorption band at 4950 Å, but such a light curve was not seen on another conjunction in 1992. It seems that the eclipsing phenomena are detectable only under favourable conditions. An eclipse may be difficult to detect at the quiescent stage, because the hot component is much fainter than the M-type giant. The light variation due to an eclipse in such conditions could be hidden by the irregular light variation of the M-type giant itself. On the other hand, the luminosity of the hot component during the active stage could be due mainly to free-free emission from the ejected circumstellar matter. Such a radiation source is likely variable and more extended than the M-type giant. Therefore, an eclipse may be difficult to detect during the active stage as well. It is possible that an eclipse by the M-type giant could be detectable when the hot component has medium activity.

An eclipse with the period of about 15 years by the third component began at the end of May 1999: ~JD2451300 (e.g. Eyres et al. 2002; Skopal et al. 2002; Burmeister & Leedjärv 2009). The luminosity of the hot component (Fig. 20) as well as the intensities of the emission lines of Hβ and Fe II (Fig. 2) decreased during the eclipse. Hinkle et al. (1993) supposed the third component to have been a G-type dwarf, while Skopal et al. (1996b) suggested an M-type giant. The eclipsing phenomena, however, suggested that the third component was much more extended than the M-type giant in the inner binary, because the well extended hot component and the emitting regions of Hβ and Fe II were eclipsed. The third component was probably surrounded by extended obscuring matter which was likely semi-transparent, because the spectrum of the M-type giant was well seen during the eclipse. The third component in CH Cyg seems to be similar to the invisible secondary component in the long-period eclipsing binary ϵ Aur (e.g. Ferluga 1990; Carroll et al. 1991). Recently, detailed analyses of the structure of the secondary component in ϵ Aur have been made (e.g. Peterson & Stencel 2015; Stencel et al. 2015), but its thickness is still not well known. The obscuring matter around the third component should have a large thickness, because the hot component in the active stage, which was probably more extended than the M-type giant, was almost totally eclipsed (Fig. 20). On the other hand, the emitting region of the Hβ line seems to have been partly eclipsed, because its intensity decreased during the eclipse (Fig. 2). The emitting regions of the lines of [O III] 5007 and [Fe II] 4814 seems to have been more extended than the third component, because the effect of the eclipse was small (Fig. 3). Detailed studies of the structure of the third component are awaited.

6. Discussion and summary

Taylor et al. (1986) found expanding nebulosity with velocities of the order of 1000 km s^{-1} around CH Cyg. Successive works have confirmed their result and further mass ejections were observed during later active stages (Solf 1987; Corradi et al. 2001; Crocker et al. 2001; Eyres et al. 2002; Karovska et al. 2010). The images of the expanding nebulosity suggested that large-scale mass ejections lasted a long time in the polar directions. Such mass ejections could be explained with a model of bipolar outflows from an accretion disc. On the other hand, the highly blueshifted broad absorption components of H I and He I lines on our spectra suggest that high-velocity and rapidly variable mass ejections occurred along the line of sight, that is to say along the orbital plane, because CH Cyg is an eclipsing binary.

The absorption components redshifted by 10–15 km s^{-1} of Na I and Fe II lines coexisted with the high-velocity outflow (~1000 km s^{-1}) during the active stage. This phenomenon might have been related to the inner disc inflow expected in wind-compressed accretion discs (Owocki et al. 1994). In contrast to the bipolar mass outflows during previous active stages, equatorial mass ejections rather similar to those of Be stars seem to have occurred during the active stage from 1998 to 2000. Corradi et al. (2001) obtained an image of CH Cyg by the HST on 1999 October 1, that is, about 250 days after the epoch of the high-velocity mass ejections (Sect. 3.2). They found two small knots of nebulosity detached about 100 AU away from the central star. The distance of 100 AU agrees with the travel length of ejecta with a velocity of the order of 1000 km s^{-1} in 250 days. Small-scale mass ejections seem to have occurred also in the polar direction at that time.

The radial velocities of the AVab seem to have represented the orbital motion of the hot component. If this is the case, our results lend support to the orbital period of about 750 days for the symbiotic binary system, because the mass of the hot component would be expected to exceed the Chandrasekhar limit by the orbital period of 15 years. The masses of the hot component and the M-type giant are estimated to be $M_1 = 0.32 \pm 0.02\ M_\odot$ and $M_2 = 4.6 \pm 0.2\ M_\odot$, respectively, for the circular orbit. If the inner binary has the elliptical orbit by $e = 0.33$ (Hinkle et al. 2009), the masses are $M_1 = 0.21 \pm 0.01\ M_\odot$ and $M_2 = 2.2 \pm 0.1\ M_\odot$. We are still unable to determine the type of the orbit with our spectroscopic data. The separation between the M-type giant and the hot component is estimated to be about 6 mas in the case of the circular orbit which is consistent with 6–8 mas obtained using infrared interferometry (Pedretti et al. 2009). The mass transfer in the binary system is probably due to a soft Roche lobe overflow.

There should have been an eclipse of the hot component by the M-type giant in the inner binary around JD2451179 (in the case of a circular orbit) or JD2451095 (in the case of an elliptical orbit), but a clear light curve of the eclipse was not seen (Fig. 20). The luminosity of the hot component in the active stage may have been due mainly to free-free emission from the ejected circumstellar matter which was likely much more extended than the M-type giant. This is probably the reason why the eclipses with the period of about 750 days were not detected in the active stages (Skopal et al. 1996b, and this paper). Another eclipse with the period of 15 years by the third component began at the end of May 1999 during which the hot component as well as the emitting regions of the Hβ and Fe II 5018 lines were eclipsed (Figs. 2 and 20). Therefore, the obscuring matter around the third component should have been much more extended than the M-type giant. The obscuring matter was likely semi-transparent,

because the spectrum of the M-type giant was well seen during the eclipse. The third component in CH Cyg appears to be similar to the secondary component in the long-period eclipsing binary ϵ Aur.

The flare-up of the emission line of [O III] 5007 at the quiescent stage in May 1997 (Fig. 3) coincided with the increase in the fluxes in the radio wavelength region (Karovska et al. 1998). These phenomena, however, were not related to an active stage. Did CH Cyg heave a sigh?

Acknowledgements. I am grateful to M. Kato and I. Hachisu for the useful discussions and suggestions.

References

Balega, I. I., Balega, Yu. Yu., Maksimov, A. F., et al. 2007, Astrophys. Bull., 62, 339
Burmeister, M., & Leedjärv, L. 2009, A&A, 504, 171
Carroll, S. M., Guinan, E. F., McCook, G. P., & Donahue, R. A. 1991, ApJ, 367, 278
Contini, M., Angeloni, R., & Rafanelli, P. 2009a, Astron. Nachr, 330, 816
Contini, M., Angeloni, R., & Rafanelli, P. 2009b, A&A, 496, 759
Corradi, R. L. M., Munari, U., Livio, M., et al. 2001, AJ, 560, 912
Crocker, M. M., Davis, R. J., Eyres, S. P. S., et al. 2001, MNRAS, 326, 781
Deutsch, R. J. S. 1964, Ann. Rep. Mt. Wilson and Palomar Obs., 11
Eyres, S. P. S., Bode, M. F., Skopal, A., et al. 2002, MNRAS, 335, 526
Ferluga, S. 1990, A&A, 238, 270
Hinkle, K. H., Fekel, F. C., Johnson, D. S., & Scharlach, W. W. 1993, AJ, 105, 1074
Hinkle, K. H., Fekel, F. C., & Joyce, R. 2009, ApJ, 692, 1360
Iijima, T., Strafella, F., Sabbadin, F., & Bianchini, A. 1994, A&A, 283, 919
Iijima, T. 1998, MNRAS, 297, 77
Karovska, M., Carilli, C. L., & Mattei, J. A. 1998, JAAVSO, 26, 97
Karovska, M., Gaetz, T. J., Carilli, C. L., et al. 2010, ApJ, 710, L132
Mikolajewska, J. Balega, Yu., Hofmann, K.-H., & Weigelt, G. 2010, MNRAS, 403, L21
Mikolajewski, M., Mikolajewska, J., & Khudyakova, T. N. 1990, A&A, 235, 219
Moore, C. E. 1959, A Multiplet Table of Astrophysical Interest (Washington DC: US Dept. of Commerce, Office of Technical Services)
Munari, U., Yudin, B. F., Kolotilov, E. A., & Tomov, T. V. 1996, A&A, 311, 484
Owocki, S. P., Cranmer, S. R., & Blondin J. M. 1994, ApJ, 424, 887
Pedretti, E., Monnier, J. D., Lacour, S., et al. 2009, MNRAS, 397, 325
Peterson III, R. L., & Stencel, R. E. 2015, ApJ, 789, 11
Skopal, A., Bode, M. F., Bryce, M., et al. 1996a, MNRAS, 282, 327
Skopal, A., Bode, M. F., Lloyd, H. M., & Tamura, S. 1996b, A&A, 308, L9
Skopal, A., Bode, M. F. Crock, M. M., et al. 2002, MNRAS, 282, 1109
Skopal, A., Bode, M. F. Lloyd, H. M., & Drechsel, H. 1998, A&A, 331, 224
Sokoloski, J. L., & Kenyon, S. J. 2003, ApJ, 584, 1027
Solf, J. 1987, A&A, 180, 207
Stencel, R. E., Baltherwick, R. D., & Geballe, T. R. 2015, AJ, 149, 109
Taylor, A. R., Seaquist, E. R., & Mattei, J. A. 1986, Nature, 319, 38
Tomov, T., Kolev, D., Munari, U., & Antov, A. 1996, MNRAS, 278, 542
van Leeuwen, F. 2007, Hipparcos, the New Reduction of the New Raw Data, Astroph. and Space Sci. Library (Berlin: Springer), Vol. 250
Wallerstein, G., Munari, U., Siviero, A., Dallaporta, S., & Dalmeri, I. 2010, PASP, 122, 12
Yamashita, Y., & Maehara, H. 1979, PASJ, 31, 307
Yoo, K. H. 2007, New Astron. 12, 569

Appendix A: Additional table

Table A.1. A log of spectroscopic observations of CH Cyg.

Date yy/mm/dd	No.	UT	Exp s	Inst.	Sp. range nm	JD 24-	Phase
95/10/16	1107	19:56	600	camVI	411–510	50007.334	0.449
95/10/25	1234	19:10	600	camVI	412–511	50016.302	0.461
95/11/20	1436	19:55	600	camVI	422–537	50042.333	0.496
95/11/21	1465	20:09	600	camVI	411–510	50043.343	0.497
95/11/23	1494	20:09	600	camVI	412–511	50045.343	0.500
95/11/24	1530	20:00	600	camVI	411–510	50046.337	0.501
95/12/10	1567	18:17	600	camVI	411–510	50062.265	0.522
95/12/19	1586	18:46	600	camVI	411–510	50071.286	0.534
96/01/19	1652	5:06	600	camVI	412–511	50101.716	0.574
96/02/01	1679	5:26	300	camVI	411–510	50114.728	0.591
96/02/08	1699	5:12	600	camVI	411–510	50121.720	0.601
96/02/15	1744	4:38	600	camVI	411–510	50128.697	0.610
96/03/02	1802	3:39	600	camVI	411–510	50144.656	0.631
96/03/29	21569	3:59	300	BC600	397–510	50171.668	0.667
96/06/06	22004	23:05	300	BC600	395–508	50241.464	0.759
96/06/11	2033	1:47	600	camVI	411–510	50245.578	0.764
96/09/07	22694	23:54	900	ech	433–689	50334.501	0.882
97/01/29	23219	4:55	600	ech	451–710	50477.708	0.071
97/01/30	23269	4:02	600	ech	451–710	50478.672	0.073
97/02/10	23510	5:05	300	BC600	394–507	50489.714	0.087
97/02/21	23794	3:32	360	ech	460–710	50500.649	0.102
97/03/29	24451	3:16	600	ech	460–710	50536.640	0.149
97/03/31	24488	3:16	600	ech	460–710	50538.640	0.152
97/04/01	24525	1:43	600	ech	460–710	50539.575	0.153
97/04/03	2114	3:26	600	camVI	410–509	50541.647	0.156
97/05/14	25122	1:55	300	BC600	398–511	50582.582	0.210
97/05/19	2147	1:05	600	camVI	411–510	50587.549	0.217
97/05/30	25354	1:27	600	ech	460–710	50598.564	0.231
97/07/01	25421	1:25	600	ech	460–710	50630.563	0.274
97/07/29	2213	22:51	600	camVI	410–509	50659.456	0.312
97/08/13	2241	23:13	600	camVI	411–510	50674.471	0.332
97/09/19	2254	21:06	600	camVI	411–510	50711.383	0.381
97/09/22	2268	22:00	600	camVI	411–510	50714.420	0.385
97/09/24	2300	22:42	600	camVI	411–510	50716.449	0.387
97/09/25	2326	21:49	600	camVI	411–510	50717.413	0.389
97/09/26	2351	22:49	600	camVI	411–510	50718.454	0.390
97/11/13	2370	17:54	600	camVI	411–510	50766.249	0.453
97/11/14	2387	18:33	600	camVI	411–510	50767.276	0.455
97/11/16	2400	19:10	600	camVI	411–510	50769.302	0.457
97/11/20	2438	20:32	600	camVI	411–510	50773.359	0.463
97/11/21	2442	18:12	600	camVI	411–510	50774.262	0.464
98/01/07	2486	17:56	900	camVI	411–510	50821.253	0.526
98/02/06	2523	5:15	300	camVI	412–511	50850.721	0.565
98/05/10	28406	22:53	600	ech	433–689	50944.457	0.689
98/06/14	28547	1:59	600	ech	433–689	50978.586	0.734
98/07/09	28650	23:45	600	ech	433–689	51004.493	0.768
98/08/09	28874	23:43	180	ech	433–689	51035.489	0.809
98/08/10	28883	1:23	180	ech	433–689	51035.559	0.809
98/08/12	28924	23:44	180	ech	433–689	51038.490	0.813
98/08/21	2600	0:05	300	BC600	388–506	51046.505	0.824
98/09/08	2694	22:18	300	BC600	382–500	51065.431	0.849
98/10/10	2802	23:31	300	BC600	399–517	51097.482	0.891
98/10/12	2821	20:26	120	BC600	398–515	51099.352	0.894
98/10/15	2848	21:40	180	BC600	398–515	51102.404	0.898

Notes. T_0 = 2446643.66, period = 756.0 days. UT: Universal time at start of exposure. BC600: Boller Chivens spectrograph with a 600 groove mm^{-1} grating. BC1200: Boller Chivens spectrograph with a 1200 groove mm^{-1} grating.

Table A.1. continued.

Date yy/mm/dd	No.	UT	Exp s	Inst.	Sp. range nm	JD 24-	Phase
98/11/17	3245	17:43	300	BC600	395–512	51135.240	0.941
98/11/28	30243	19:40	600	ech	433–689	51146.323	0.956
98/11/29	3428	17:50	1200	BC1200	450–511	51147.250	0.957
98/12/05	3452	17:42	600	BC1200	445–506	51153.241	0.965
98/12/09	3470	19:32	600	BC600	401–519	51157.317	0.970
98/12/13	30985	18:06	1200	ech	451–711	51161.261	0.976
98/12/14	31008	18:54	600	ech	451–711	51162.291	0.977
98/12/15	31033	19:02	300	ech	451–711	51163.295	0.978
99/01/04	3572	18:14	300	BC600	396–514	51183.262	0.005
99/01/06	3600	18:07	300	BC600	395–513	51185.257	0.007
99/01/13	3665	17:38	600	BC1200	454–514	51192.238	0.017
99/01/25	3876	4:39	600	BC1200	445–506	51203.697	0.032
99/01/26	3908	5:24	300	BC600	398–515	51204.727	0.033
99/01/30	31795	5:20	600	ech	433–689	51208.726	0.038
99/02/03	31921	4:30	300	ech	433–689	51212.689	0.044
99/02/13	32041	4:29	300	ech	433–689	51222.689	0.057
99/02/17	32134	3:57	300	ech	433–689	51226.666	0.062
99/02/26	32280	3:38	600	ech	433–689	51235.655	0.074
99/03/08	4177	2:42	300	BC600	395–512	51245.614	0.087
99/03/14	32455	3:00	300	ech	433–689	51251.627	0.095
99/03/15	32475	2:47	300	ech	433–689	51252.618	0.097
99/04/02	32694	2:33	300	ech	433–689	51270.608	0.120
99/04/03	32725	1:44	300	ech	433–689	51271.574	0.122
99/04/04	32750	1:44	300	ech	433–689	51272.574	0.123
99/06/04	32895	0:33	600	ech	433–689	51333.526	0.204
99/06/05	32913	1:37	300	ech	460–710	51334.569	0.205
99/06/07	32924	1:23	300	ech	433–689	51336.559	0.208
99/06/22	4458	0:59	900	BC600	400–518	51351.546	0.227
99/09/13	4757	19:55	300	BC600	400–518	51435.332	0.338
99/09/14	4793	22:06	600	BC600	394–512	51436.424	0.340
99/09/21	4806	20:59	600	BC600	398–515	51443.378	0.349
99/09/22	4815	23:44	600	BC600	400–518	51444.492	0.350
99/09/28	33179	22:20	360	ech	433–689	51450.433	0.358
99/10/27	4905	22:59	600	BC600	400–518	51479.461	0.397
99/11/08	5004	21:50	300	BC600	399–516	51491.412	0.412
99/11/28	5371	19:44	300	BC600	415–533	51511.324	0.439
99/11/30	5423	19:36	300	BC600	406–524	51513.318	0.441
00/01/26	34045	5:18	600	ech	433–689	51569.724	0.516
00/02/21	34301	3:43	600	ech	433–689	51595.658	0.550
00/03/16	34352	2:43	900	ech	433–689	51619.618	0.582
00/04/26	34656	0:27	300	ech	433–689	51660.520	0.636
00/05/15	34745	2:39	300	ech	433–689	51679.612	0.661
00/05/16	34764	2:41	300	ech	433–689	51680.614	0.663
04/09/10	17657	23:35	300	BC600	407–525	53259.484	0.751
04/12/23	18069	17:36	600	BC600	399–517	53363.237	0.888